



ELSEVIER

Contents lists available at SciVerse ScienceDirect

## Commun Nonlinear Sci Numer Simulat

journal homepage: [www.elsevier.com/locate/cnsns](http://www.elsevier.com/locate/cnsns)

## Effect of noise on the reinjection probability density in intermittency

Ezequiel del Rio<sup>a,\*</sup>, Miguel A.F. Sanjuán<sup>b</sup>, Sergio Elaskar<sup>c</sup><sup>a</sup> Departamento de Física Aplicada, ETSI Aeronáuticos, Universidad Politécnica de Madrid, Cardenal Cisneros 3, 28040 Madrid, Spain<sup>b</sup> Departamento de Física, Universidad Rey Juan Carlos, Tulipán s/n, 28933 Móstoles, Madrid, Spain<sup>c</sup> Departamento de Aeronautica, Facultad de Ciencias Exactas, Físicas y Naturales, Universidad Nacional de Córdoba, Avenida Velez Sarfield, 1611, 5000 Córdoba, Argentina

## ARTICLE INFO

## Article history:

Received 29 September 2011

Received in revised form 15 January 2012

Accepted 18 January 2012

Available online 2 February 2012

## Keywords:

Chaos

Intermittency

One-dimensional map

## ABSTRACT

This paper analyzes the effect of noise in type-II and type-III intermittency, with respective local Poincaré maps of  $x_{n+1} = (1 + \varepsilon)x_n + (1 - \varepsilon)x_n^3$  and  $x_{n+1} = -(1 + \varepsilon)x_n - ax_n^3$  ( $a > 0$ ). We develop a method to obtain the noisy reinjection probability density (NRPD), which basically consists in extending a recent procedure used to derive the noiseless reinjection probability density (RPD). Our approach also provides information to accurately describe the noiseless system. We also derive the probability density of the laminar length. Our analytical results show a good agreement with numerical simulations. Finally, we have also found that, for large values of the instability parameter  $\varepsilon$ , the characteristic relations approach the associated ones to the noiseless intermittency. However, for low values of the instability parameter  $\varepsilon$ , the characteristic relations reach a saturation level that depends on the NRPD.

© 2012 Elsevier B.V. All rights reserved.

## 1. Introduction

Intermittency is a particular route to deterministic chaos, where a transition between laminar and chaotic phases occurs. Pomeau and Maneville introduced the concept of intermittency in connection with the Lorenz system in [1,2]. The intermittency phenomenon appears in some physical systems as in the Lorenz system, periodically forced nonlinear oscillators, Rayleigh–Bénard convection, DNLS equation and in turbulence processes in hydrodynamics, among many others. It is very important to properly characterise the intermittency phenomenon, especially in those fields, whose exact governing equations are partially unknown, as it happens in Economics and Medicine [3,4]. Pomeau classified the intermittency cases into three types called I, II and III [5]. In all the cases, a fixed point of the system becomes unstable for positive values of a given parameter  $\varepsilon$ . The local Poincaré maps of type-II and type-III intermittencies are  $x_{n+1} = (1 + \varepsilon)x_n + (1 - \varepsilon)x_n^3$  and  $x_{n+1} = -(1 + \varepsilon)x_n - ax_n^3$  ( $\varepsilon, a > 0$ ) respectively. Another condition for a one-dimensional map  $F(x)$  to possess intermittency is to have a *global* reinjection mechanism mapped back into the system from the chaotic zone into the *local* laminar one.

This mechanism is properly described by the corresponding reinjection probability density (RPD), which is determined by the chaotic dynamics of the system itself. Only in a few cases it is possible to get an analytical expression for the RPD, hence different approximations have been used. The most common approximation has been to consider the RPD as a constant. However, recently it has been introduced a more general RPD that includes the uniform reinjection as a particular case [6,7].

Since the noise is always present in nature, it is of a fundamental importance to know the effect of noise on the intermittency phenomenon. There are many papers devoted to study such an effect, by means of the renormalisation group analysis [8] or by using the Fokker–Plank equation [9–12]. Many researches devoted to the noise on the local Poincaré map have been published so far, but in spite of the importance of the RPD, there is no study focused on the effect of noise on the RPD as far as

\* Corresponding author. Tel.: +34 913366640; fax: +34 913366303.

E-mail address: [ezequiel.delrio@upm.es](mailto:ezequiel.delrio@upm.es) (E. del Rio).

the authors know. It is clear that noise affects the whole region where the system dynamics takes place, hence it demands an investigation of the effect of noise on the chaotic region and the changes that it produces on the RPD. In this paper, we report on an analytical approach to the noise reinjection probability density (NRPD). To do this, we use a recently proposed methodology to determine the RPD in maps having intermittency [6,7], to compute NRPD in terms of the RPD.

On the other hand, to study the local effect of the noise, it is usually assumed that the noise strength  $\sigma$  is much smaller than  $\varepsilon$ , ( $\sigma \ll \varepsilon$ ). This seems to be somewhat an artificial assumption since in real systems it is difficult or even impossible to change the level of noise, that is, the value of  $\sigma$  is fixed from outside the system, so that in the limit  $\varepsilon \rightarrow 0$  the system will be in a parameter region where the last assumption cannot be applied. In this work we consider a situation where this assumption should not be necessary.

To apply our theory we use two models of one-dimensional maps, one for the type-II and another one for the type-III intermittency [6,7,13]. For the type-II intermittency case, we introduce an additive external noise

$$x'_{n+1} = \begin{cases} F(x_n) + \sigma \xi_n & x_n \leq x_r, \\ (F(x_n) - 1)^\gamma + \sigma \xi_n & x_n > x_r, \end{cases} \tag{1}$$

where  $\xi_n$  is a uniform distributed noise with  $\langle \xi_m, \xi_n \rangle = \delta(m - n)$  and  $\langle \xi_n \rangle = 0$ ,  $\sigma$  is the noise strength and  $F(x) = (1 + \varepsilon)x_n + (1 - \varepsilon)x_n^3$ , where  $x_r$  is the root of the equation  $F(x_r) = 1$  (see Fig. 1). Note that the function  $F(x)$  maps the interval  $[0, 1]$  onto itself, but due to the noise, the value of  $x'_{n+1}$  may be mapped out of the unit interval. Hence, to keep  $x'_{n+1}$  in the unit interval we define the map as follows

$$x_{n+1} = \begin{cases} |x'_{n+1}| & x'_{n+1} \leq 1, \\ |x'_{n+1}| - 2\text{mod}(|x'_{n+1}|, 1) & x'_{n+1} > 1. \end{cases} \tag{2}$$

Note that  $x_{n+1} = x'_{n+1}$  for  $x'_{n+1} \in [0, 1]$ . The value  $x'_{n+1}$  is reflected around  $x' = 0$  coming back into the positive values for  $x'_{n+1} < 0$ . For  $x'_{n+1} > 1$ , a similar effect around  $x' = 1$  getting  $x_{n+1} < 1$  is produced.

In the noiseless case,  $\sigma = 0$ , the critical point  $x = 0$  is an unstable point for  $\varepsilon > 0$ , then the iterated points  $x_n$  of a starting point close to the origin, increase in a process driven by parameter  $\varepsilon$ . When  $x_n$  becomes larger than  $x_r$ , a chaotic burst occurs that will be interrupted when  $x_n$  is again mapped into the laminar region. For a point close to  $x_r$  and lying on the curve corresponding to  $\gamma = 2$ , the reinjection mapping into the laminar region is illustrated in Fig. 1 by a dashed arrow between two solid lines. This trajectory, due to the noise, may spread over a region indicated by the solid lines, whereas the dashed arrow refers to the noiseless map.

Note that according to Eq. (1) the reinjection process is governed by a power law  $(\cdot)^\gamma$  driven by the parameter  $\gamma$ .

Concerning type-III intermittency, we use the map

$$x_{n+1} = -(1 + \varepsilon)x_n - ax_n^3 + dx_n^6 \sin(x_n) + \sigma \xi_n, \tag{3}$$

where  $-(1 + \varepsilon)x_n - ax_n^3$  ( $a > 0$ ) is the standard local map for type-III intermittency, whereas the term  $dx_n^6 \sin(x_n)$  ( $d > 0$ ) provides the reinjection mechanism into the laminar region around the critical point  $x = 0$ . This mechanism, different from the power law used in the case for type-II intermittency, has been chosen to apply our method to different nonlinearities.

The RPD function, denoted here by  $\phi(x)$ , determines the statistical behaviour of the intermittency phenomenon. However, it is not a simple task to establish the RPD by using experimental or numerical information, hence in order to investigate the RPD we extend in this work the proposed method in our previous papers [6,7]. In this approach we realised that the key point to determine the RPD is to evaluate, instead of the RPD itself, the following function

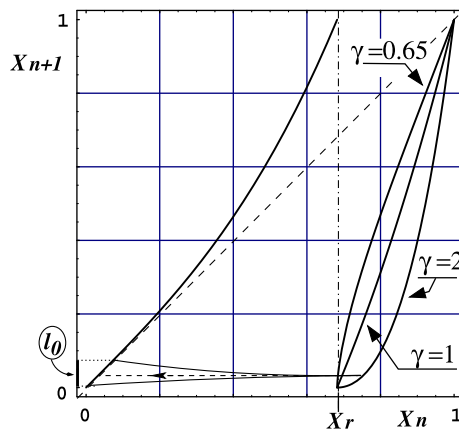


**Fig. 1.** Map of Eq. (1) with  $\sigma = 0$  and  $\varepsilon = 10^{-3}$ . We have used here three values of  $\gamma$  as indicated. For  $\gamma = 2$ , the dashed arrow indicates the noiseless trajectory going into the laminar region. For  $\sigma \neq 0$ , that trajectory should be shifted to end inside the interval  $I_0$ .

$$M(x) = \begin{cases} \frac{\int_0^x \tau \phi(\tau) d\tau}{\int_0^x \phi(\tau) d\tau} & \text{if } \int_0^x \phi(\tau) d\tau \neq 0, \\ M(x) = 0 & \text{if } \int_0^x \phi(\tau) d\tau = 0 \end{cases} \quad (4)$$

defined over the interval  $[0, c]$ , where the parameter  $c$  specifies the upper limit for the laminar region. As  $M(x)$  is defined by means of integrals, it is easier to compute than  $\phi(x)$ , and also the effects coming from the statistical fluctuations are reduced, even for a relatively low number of data or a high noise level. Moreover, note that for a given value of  $x$ ,  $M(x)$  is the average of reinjection points in the interval  $(0, x)$ , hence, even for a non very extensive data series obtained from  $N$  iterations of the map, it is possible to obtain a good approximation for the function  $M(x)$ . Firstly, we sort the reinjections points according to the relation  $x_j < x_{j+1}$  and finally, a simple estimation of the function  $M(x)$  is obtained by means of

$$M(x_i) \approx \frac{\sum_{j=1}^i x_j}{i}, \quad (5)$$

which has been used in this work to evaluate the function  $M(x)$  instead of using the definition Eq. (4).

To numerically evaluate the RPD and the NRPD, we make  $N = 10^6$  iterations of the map and select the reinjected points back from the chaotic burst into the laminar region. The number of reinjected points depends on the map and the specific set of parameter values chosen to make the iterations. The laminar region is divided into small intervals, ranging from 100 to 1000 looking for the best result, and finally we evaluate the average over the reinjection points in each interval. Note that to apply the approximation Eq. (5), we need a value of  $N$  several times smaller than the value needed to compute the RPD or NRPD. In all cases considered here, the value  $N = 10^5$  would be enough.

Now we briefly summarise the previous results [6,7] on noiseless intermittency useful to investigate the effect of noise on the reinjection probability density. For a wide class of maps having type-II or type-III intermittency, the function  $M(x)$  can be approximated by the linear function

$$M(x) = m(x - x_i) + x_i, \quad (6)$$

where the unstable fixed point  $x_i$ , here takes the value  $x_i = 0$ . After using the definition, Eq. (4), we obtain the corresponding reinjection probability density as

$$\phi(x) = bx^\alpha, \quad \text{with } \alpha = -\frac{1-2m}{1-m}, \quad (7)$$

where  $b$  is determined by the normalisation condition

$$\int_0^c bx^\alpha dx = 1. \quad (8)$$

Assuming  $\alpha > -1$ , that is  $0 < m < 1$ , this last integral converges, and consequently

$$b = \frac{\alpha + 1}{c^{\alpha+1}} = \frac{m}{1-m} c^{\frac{m}{1-m}}. \quad (9)$$

According to Eq. (7), and for the particular value  $m = 1/2$ , we recover the most common approach  $\phi(x) \approx \text{const.}$  considered in the literature.

## 2. Effect of noise on the RPD

In previous papers we have used the function  $M(x)$  as a useful tool to study the RPD. In the noisy case, we also use this function to investigate the new NRPD in systems with type II and type III intermittency. Now we describe the case of type II intermittency.

In this case, we evaluate the function  $M(x)$  for the map Eqs. (1) and (2) in the noisy and noiseless cases, as shown in Fig. 2. Note that the function  $M(x)$  looks like a smooth function even in the noisy case ( $\sigma = 0.03$ ), due to the fact that the integrals in the definition of  $M(x)$  filter the noise. Whereas in the noiseless case, the function  $M(x)$  can be approximated by a linear function [6], in the noisy case the function  $M(x)$  can be approximated by a piecewise linear function with different slopes, on each side of  $x_0$  (see Fig. 2). The value  $x_0$  depends on the noise strength  $\sigma$ . In the region  $x < x_0$  the slope of  $M(x)$  approaches 1/2, as we expect for the uniform reinjection. Note however that in the noiseless case there is no uniform reinjection, but there is a power law given by Eq. (7). On the side  $x_0 < x$ , the slope of  $M(x)$  is different from the 1/2 taking a value close to the corresponding noiseless value. Note that for  $\gamma = 0.65$  (the case  $\gamma = 2$  will be considered at the end of this section) in the noisy case the slope is  $m \approx 0.61$  which is very close to the noiseless case  $m \approx 0.60$ . Hence in that region the NRPD must be similar to the RPD function. This means that, by the analysis of the noisy data, we can predict the RPD function for the noiseless case. To do this, we proceed like in the noiseless case [6,7], but considering only the data on the right side of  $x_0$  in Fig. 2. That is, by least mean square analysis we can calculate the slope  $m$  in Eq. (6), that determines the reinjection function given by Eq. (7). This is shown in Fig. 3 for the same values of  $\gamma$  than in Fig. 2. That is, in Fig. 3(a), we have  $\gamma < 1$  so that  $\lim_{x \rightarrow 0} \phi(x) = 0$  and in Fig. 3(b), we have  $\gamma > 1$  so that  $\lim_{x \rightarrow 0} \phi(x) = \infty$  [6]. The result displayed in this figure shows that, in both cases, from the function  $M(x)$  evaluated in the noisy cases it is possible to approximate the RPD in the noiseless case.

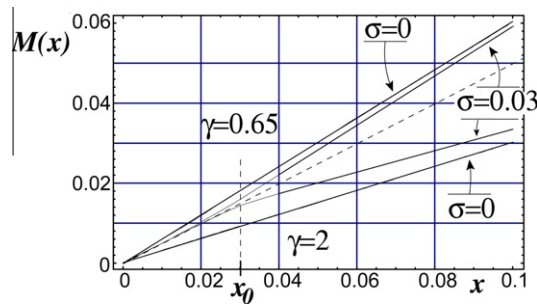


**Fig. 2.** Numerical simulations of the function  $M(x)$  for the map Eqs. (1) and (2) computed using Eq. (5). The dashed line with slope 1/2 shows the uniform reinjection case. The lines above the dashed one correspond to  $\gamma = 0.65$  for two values of the noise strength as indicated. The same values of noise strength is used for the two lines below the dashed one, that correspond to  $\gamma = 2$ . For all the cases  $\varepsilon = 0.001$  is fixed and  $c = 0.1$ . The solid lines show the corresponding least mean square fit, very close to the numerical simulations.

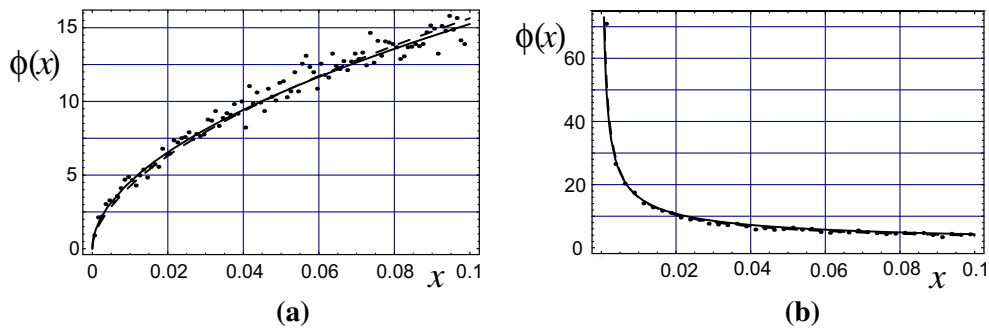


**Fig. 3.** RPD for the map Eqs. (1) and (2). Dots corresponds to numerical computation for  $\sigma = 0$  whereas solid lines correspond to Eq. (7) using two values of  $m$  obtained by fitting data with  $\sigma = 0$  (dashed line) and  $\sigma \neq 0$  (solid line). The values of the parameter  $\gamma$  are the same that in Fig. 2. (a) In this case  $\gamma < 1$ . We fix  $c = 0.1$ ,  $\gamma = 0.65$ ,  $\sigma = 0.03$  and  $\varepsilon = 0.001$ . (b) In this case  $\gamma > 1$ . We fix  $c = 0.1$ ,  $\gamma = 2$ ,  $\sigma = 0.01$  and  $\varepsilon = 0.001$ .

It is important to note that whereas the noise is applied to the whole map, the function  $M(x)$  evidences that, on the right side of  $x_0$  of Fig. 2, the reinjection function is robust against the noise but on the left side of  $x_0$ , the noise changes the RPD approaching it to the uniform reinjection, at least locally around  $x = 0$ .

We will find a similar scenario in type-III intermittency, but in that case, the value of  $x_0$  is bigger. We use the map Eq. (3) to illustrate the noise effect in the type-III intermittency. As in the previous case, we start with a numerical evaluation of the function  $M(x)$  by using the approximation given by Eq. (5). This is shown in Fig. 4 for two values of the noise strength  $\sigma$  together with the noiseless case  $\sigma = 0$ . As in Fig. 2, for values close to the origin (on the left of the arrows), the function  $M(x)$  approaches  $M(x) \approx 0.5x$ , but for points on the right hand side of the arrows we have  $M(x) \approx mx$  where the slope  $m$  is similar as to in the noiseless map.

Note however, that here the transition from the 0.5 slope to a slope close to the noiseless case takes place for bigger values of  $x_0$  than in the type-II case. That is, the effect of noise on the function  $M(x)$  is stronger than in the previous case.

As the three values of  $m$  estimated for data in Fig. 4 are similar, we can use each of them to describe the RPD of the noiseless case. Hence, as in the type-II intermittency we can estimate the behaviour of the noiseless map from noisy data, as shown in Fig. 5.

### 2.1. NRPD in type II intermittency

To get an analytical expression for the NRPD, denoted here by  $\Phi(x)$ , we analyse the effect of noise on the reinjection trajectories, as it is sketched in Fig. 1. In such a figure, a noiseless trajectory represented by a dashed line, is perturbed by noise. As a consequence of this, the reinjection point must be ended inside of an interval represented in Fig. 1 by  $I_0$ . That is, the noiseless density  $\phi'(x)$  should be transformed into a new density  $\Phi(x)$  according to the convolution

$$\Phi(x) = \int \phi'(y)G(x - y, \sigma)dy, \tag{10}$$

where  $G(x, \sigma)$  is the probability density of the noise term  $\sigma \xi_n$  in Eq. (1).

Whereas the function  $\phi'(x)$  is in general unknown, we have information on  $\Phi(x)$  by means of the function  $M(x)$  as was explained above. Furthermore, taking into account the convolution properties, we expect  $\Phi(x) \approx \phi'(x)$  in the region where the slope of  $\phi'(x)$  is small. On the other hand, the slope of the noisy function  $M(x)$  approaches the corresponding slope

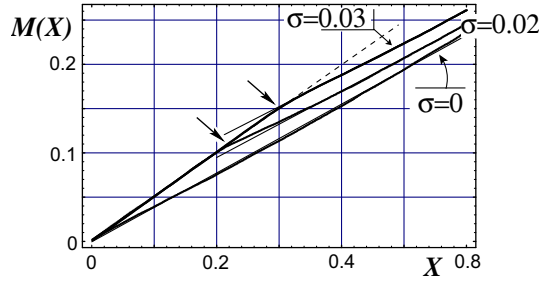


**Fig. 4.** Function  $M(x)$  for the map Eq. (3) for three different values of the noise strength as indicated. Dots correspond to the numerical evaluation of  $M(x)$  and solid lines show the corresponding least mean square fit that, according with their slopes ( $m_{(\sigma=0)} = 0.364$ ,  $m_{(\sigma=0.02)} = 0.375$  and  $m_{(\sigma=0.03)} = 0.367$ ) can be considered as parallel lines. The dashed line slope is  $1/2$  and it corresponds to a uniform reinjection. The parameters are:  $c = 0.8$ ,  $a = 1.1$ ,  $d = 1.35$ ,  $\varepsilon = 10^{-4}$ . Arrows show when  $M(x)$  change the  $1/2$  slope.

without noise, determining the density  $\phi(x)$  in the noiseless case. These facts suggest that  $\phi'(x) \approx \phi(x)$ , where  $\phi(x) = b|x|^\alpha$  is the RPD without noise, hence the parameters  $b$  and  $\alpha$  can be taken as the same values that in the noiseless case. Observe that, although the noise is applied to the complete map, the associated power law to the effect of the nonlinearity observed in the noiseless map, appears to be robust against noise. To verify this hypothesis we introduce  $\phi'(x) = b|x|^\alpha$  in Eq. (10). As noise source we used a random variable  $\xi$  in the interval  $[-1, 1]$ , hence its probability density  $G$  in Eq. (10) is given by

$$G(x, \sigma) = \frac{\Theta(x + \sigma) - \Theta(x - \sigma)}{2\sigma}, \tag{11}$$

where  $\Theta(x)$  is the Heaviside step function. Finally, after integrating Eq. (10), we get the NRPD as

$$\Phi(x) = \frac{1}{c^{1+\alpha}} \frac{(|x| + \sigma)^{1+\alpha} - \text{Sg}(|x| - \sigma) | |x| - \sigma |^{1+\alpha}}{2\sigma}, \tag{12}$$

where we denote by  $\text{Sg}(x)$  the sign function that extracts the sign from its argument. To compare Eq. (12) with the numerical simulations, we use the values of  $\alpha$  determined by the values of  $m$  obtained from Fig. 2. The results are plotted in Fig. 6 for different values of  $\sigma$ , showing a good agreement between the numerical simulations and the analytical predictions. To plot the solid lines of Fig. 6 we can use either values of  $m$  obtained from noisy data of Fig. 2, or the corresponding value from the noiseless data because both values are approximately equal. However, it is not the case when  $\gamma = 2$  and  $\sigma = 0.03$ . Here the noisy slope of  $M(x)$  is  $m_n \approx 0.268$ , so the error relative to the noiseless value (0.30) is around 10%. This error makes a similar deviation between Eq. (12) and numerical data as shown in Fig. 7 by a dashed line. Nevertheless, we can compare Eq. (12) using a noiseless value of  $m$  with the numerical noisy data. This is shown in Fig. 7 by a solid line in good agreement with the numerical simulations. This proves that the hypothesis  $\phi'(x) = b|x|^\alpha$  works well even when the high level of noise makes it significant differences between the slopes of  $M(x)$  with and without noise.

Moreover, even in this case it is possible to estimate the function  $M(x)$  for points  $x > x_p$  far enough from the critical point  $x = 0$ , that is  $x_p > x_0$  (see Fig. 2). To do this, we note that in the region  $x > x_p$  the slope of  $\phi'(x)$  is small, so according with Eq. (10) we expect  $\Phi(x) \approx \phi'(x)$ , hence by using the definition of  $M(x)$ , (Eq. (4)) we have

$$M_n(x) \approx M(x) + \frac{\int_0^x \tau(\Phi(\tau) - \phi(\tau))d\tau}{\int_0^x \phi(\tau)d\tau} \quad \text{if } x > x_p, \tag{13}$$

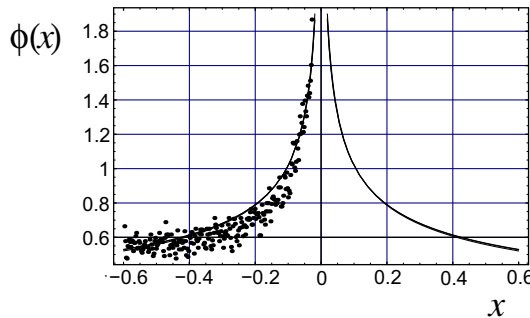


**Fig. 5.** RPD for the map Eq. (3). Dots correspond to numerical data. For clarity we have omitted the points on the right hand side. Solid lines correspond to Eq. (7) evaluated using the three values of  $m$  of Fig. 4, where the three of them are almost coincident. The parameters are:  $c = 0.6$ ,  $a = 1.1$ ,  $d = 1.35$  and  $\varepsilon = 10^{-4}$ .

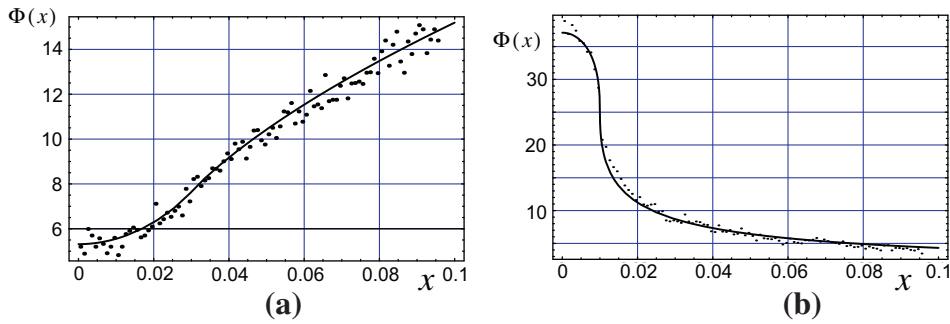


**Fig. 6.** NRPD for the map Eqs. (1) and (2) using two set of parameters: (a)  $c = 0.1$ ,  $\gamma = 0.65$ ,  $\sigma = 0.03$  and (b)  $c = 0.1$ ,  $\gamma = 2$  and  $\sigma = 0.01$ . Dots correspond to numerical data whereas the analytical approximation given by (12) is plotted as a solid line.

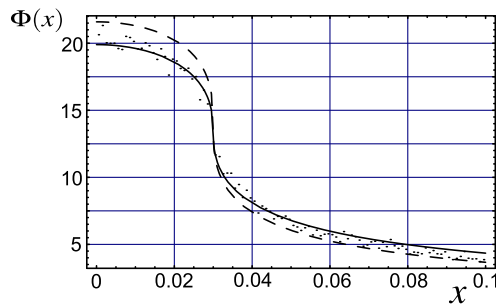


**Fig. 7.** NRPD for the map Eqs. (1) and (2) for parameters  $c = 0.1$ ,  $\gamma = 2$  and  $\sigma = 0.03$ . Dots correspond to the numerical values of NRPD. The dashed line correspond to the analytical approximation Eq. (12) using the value  $m = 0.268$ , obtained from the noisy case of Fig. 2. We also plot Eq. (12), solid line, but we used  $m = 0.30$ , as obtained from Eq. (14).

where  $M_n(x)$  and  $M(x)$  are the noisy and noiseless functions respectively and we assume that the integral in the denominator does not depend on noise. With the approximation given by Eq. (5), we get for  $x_i > x_p$

$$M(x_i) \approx M_n(x_i) - \frac{C}{l} \approx \frac{\sum_{j=1}^l x_j}{l} - \frac{C}{l}. \tag{14}$$

As  $M(0) = 0$  we can choose the value  $C$  to approximate  $M(0) \approx 0$ . In our case, the value  $C = 350$  gives the line  $M(x_i) = 0.0004 + 0.298x_i$ , with a small independent term. As we expected, this line has a slope very close to the noiseless case,  $m \approx 0.301$ . This means, that even in this case with a very high value of the noise strength, the density  $\phi(x) = b|x|^\alpha$  of the noiseless map is recovered.

### 2.2. NRPD in type III intermittency

The RPD,  $\phi(x)$ , for type-III intermittency follows a power law depending on the neighbourhood of the maximum and minimum of the map Eq. (3) [7]. The noiseless trajectory of a point starting near the maximum of the map appears in Fig. 8 as a dashed line. Because of the noise, this trajectory may spread over a region of some width, say  $l_0$ . Note that  $l_0$  will be rescaled by a suitable factor  $K$  increasing the length up to  $l_1 = Kl_0$  on the graph of the map. To get an analytical approximation for the NRPD,  $\Phi(x)$ , we consider the map Eq. (3) as a composition of the noiseless map

$$x'_n = -(1 + \varepsilon)x_n - ax_n^3 + dx_n^6 \sin(x_n) \tag{15}$$

and the new map defined as

$$x_{n+1} = x'_n + \sigma \xi_n, \tag{16}$$

by just adding a noise to the variable. Now we focus on a point  $x_n$  lying close to the maximum of the map Eq. (15). As in the type-II intermittency, if  $\rho'(x)$  is the invariant density in that region due to the map Eq. (15), the effect on this density of the map Eq. (16) can be obtained according to the convolution

$$\rho(x) = \int \rho'(\tau)G(\tau - x, \sigma)d\tau, \tag{17}$$

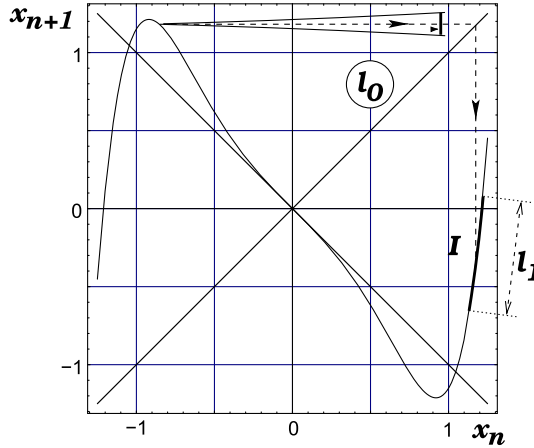


**Fig. 8.** Map of Eq. (3). Dashed line between the two solid lines indicate the effect of the map on a point near the maximum. These solid lines indicate the effect of the noisy map on the same point, that will be mapped on the interval  $I$  on the graph of the map.

where  $\rho(x)$  is the invariant density observed in the interval  $l_0$ . Contrary to the type-II case, here points on  $l_0$  are not directly mapped on the laminar region, so to get the NRPD we must propagate the density  $\rho(x)$  by the map Eq. (3). Then we propagate  $\rho(x)$  by the map Eq. (15) to reach for points in the interval  $I$

$$\rho_I(x) = \frac{dF^{-1}(x)}{dx} \rho(F^{-1}(x)) \tag{18}$$

and later, we must propagate the density  $\rho_I(x)$  by the map Eq. (16) to obtain the NRPD

$$\Phi(x) = \int \rho_I(y) G(y - x, \sigma) dy. \tag{19}$$

By using Eqs. (17) and (18), we get

$$\Phi(x) = \iint \frac{dF^{-1}(y)}{dy} \rho'(\tau') G(\tau' - F^{-1}(y), \sigma) G(y - x, \sigma) dy d\tau' \tag{20}$$

and by rescaling the dummy variable  $\tau' = F^{-1}(\tau)$  we can rewrite the last equation in a better form to be compared with the noiseless case as

$$\Phi(x) = \iint \phi(\tau) G_F(\tau, y) G(y - x, \sigma) dy d\tau, \tag{21}$$

where we use the following definitions

$$\phi(x) = \frac{dF^{-1}(x)}{dx} \rho'(F^{-1}(x)) \tag{22}$$

and

$$G_F(\tau, y) = \frac{dF^{-1}(y)}{dy} G(F^{-1}(\tau) - F^{-1}(y), \sigma). \tag{23}$$

Eq. (22) shows the effect of the noiseless map on the density  $\rho'$ . By using the aforementioned hypotheses for type-II intermittency, we can approximate  $\rho'$  by the same power law that in the noiseless map. Using the linear approximation  $F(x) \approx F(x_{-1}) + K(x_{-1} - x)$ , where  $K = dF/dx$  corresponds to the mean slope of the curve  $I$ , the density  $\phi$  in Eq. (22) can be approximated by a similar power law than  $\rho'$  [7], that is  $\phi(x) \approx b|x|^\alpha$  even in the noisy case. By considering the previous linear approximation we get for the function  $G_F(\tau, y)$

$$G_F(\tau, y) \approx G(\tau - y, K\sigma). \tag{24}$$

In our case  $K \approx 10$ , so that the density  $G(y - x, \sigma)$  in the integral (21) is very narrow as compared with the approximation for  $G_F$  given by Eq. (24), so that in the limit  $G(y - x, \sigma) \approx \delta(y - x)$ , we get for the NRPD

$$\Phi(x) = \int \phi(\tau) G(\tau - x, K\sigma) d\tau, \tag{25}$$

a expression similar to Eq. (10) obtained to describe the noise in the type-II intermittency. Hence we can proceed in the same way that in the previous case,

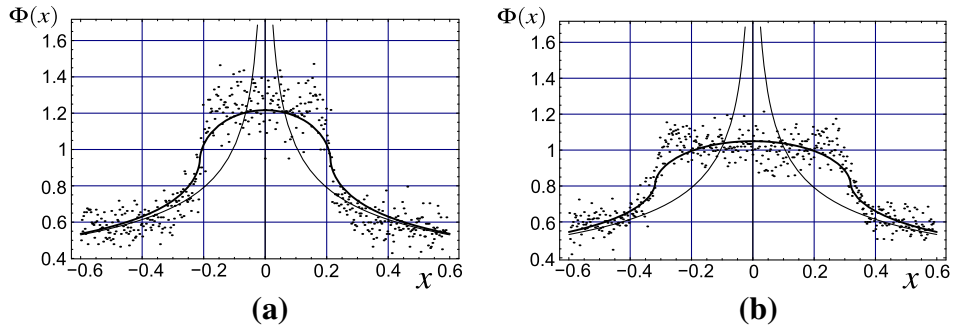


**Fig. 9.** NRPD for two values of the noise strength  $\sigma$  of Eq. (3) as following: (a)  $\sigma = 0.02$  and (b)  $\sigma = 0.03$ . Dots refer to numerical simulation whereas solid lines are the plots of the analytical approximation to NRPD given by Eq. (26). Note that to illustrate the effect of the noise, the noiseless RPD it is also plotted. As in Fig. 5, the parameters are:  $c = 0.6$ ,  $a = 1.1$ ,  $d = 1.35$  and  $\varepsilon = 10^{-4}$ .

$$\Phi(x) = \frac{1}{c^{1+\alpha}} \frac{(|x| + K\sigma)^{1+\alpha} - \text{Sg}(|x| - K\sigma)|x| - K\sigma}{2K\sigma} \tag{26}$$

Note that Eq. (26) is similar to Eq. (12) but here the factor  $K$  produces an amplification of the effect of the noise. This expression is plotted in Fig. 9 showing a good agreement with the numerical data.

### 3. Characteristic relations

A fundamental quantity related to the intermittency phenomenon is the probability density of the laminar length  $\phi_l(l)$ , where  $l$  indicates the number of iterations in the laminar region. Here, we can approximate the dynamics of the noiseless maps Eqs. (1)–(3) by the differential equation [5]

$$\frac{d|x|}{dl} = \varepsilon|x| + a|x|^3 \tag{27}$$

By solving the above equation we obtain

$$l(|x|, c) = \int_{|x|}^c \frac{dz}{\varepsilon z + a z^3} = \frac{1}{2\varepsilon} \left[ 2 \ln \left( \frac{c}{|x|} \right) - \ln \left( \frac{\varepsilon + a c^2}{\varepsilon + a x^2} \right) \right], \tag{28}$$

which is referred to a local behaviour of the map in the neighbourhood around of the unstable point. The probability of finding a laminar phase of a given length lying between  $l$  and  $l + dl$  is  $\phi_l(l)dl$  where the density  $\phi_l(l)$  is given by

$$\phi_l(l) = f \cdot \Phi(X(l, c)) \left| \frac{dX(l, c)}{dl} \right|, \tag{29}$$

where  $X(l, c)$  is  $l^{-1}(x, c)$  with respect to its first argument

$$X(l, c) = \sqrt{\frac{\varepsilon}{(a + \varepsilon/c^2)e^{2\varepsilon l} - a}} \tag{30}$$

Observe that, being aware of the symmetry of the type-III intermittency of Eq. (3), we have considered  $x > 0$  and written  $\phi(|x|) = f \cdot \phi(x)$  with  $f = 2$ , whereas for the type-II we used  $f = 1$ . Taking into account Eq. (27) and the above relations, we finally have

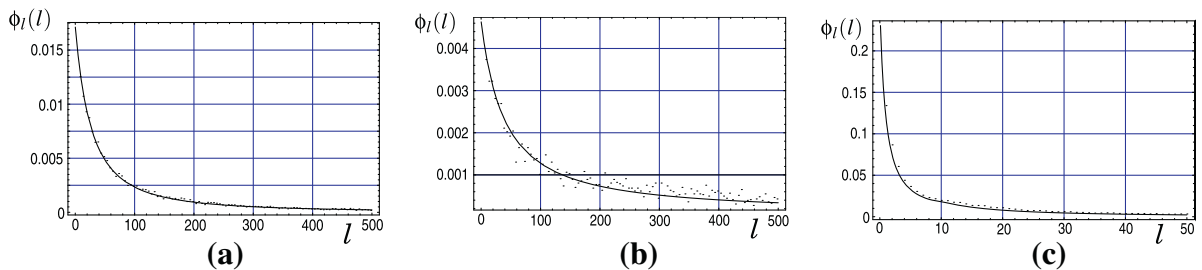


**Fig. 10.** Function  $\phi_l(l)$  (solid lines) according to Eq. (31) for maps Eqs. (1)–(3) together with the numerical values (dots). (a) Map of Eqs. (1) and (2) with  $\gamma = 0.65$ ,  $\sigma = 0.001$  and  $\varepsilon = 0.001$ , (b) map Eqs. (1) and (2) with  $c = 0.1$ ,  $\gamma = 2$ ,  $\sigma = 0.001$  and  $\varepsilon = 0.001$  and (c) map Eq. (3) with  $c = 0.6$ ,  $a = 1.1$ ,  $d = 1.35$ ,  $\sigma = 0.001$  and  $\varepsilon = 0.001$ .

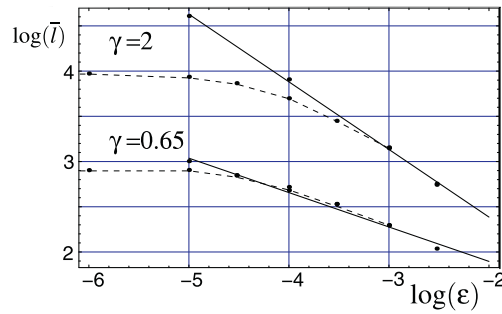


**Fig. 11.** Characteristic relations for the map Eq. (1) and (2) for  $c = 0.1$  and two values of  $\gamma$ . Dots show numerical data and solid line represents the least squares straight fitting data corresponding to  $\sigma = 0$ . For two values of  $\gamma$ , the dashed lines join the noisy data ( $\sigma = 10^{-4}$ ) reaching the corresponding saturation label for small values of  $\epsilon$ .

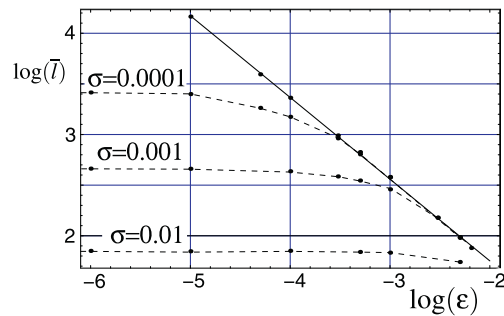


**Fig. 12.** Characteristic relations for the map Eq. (3). Dots show numerical data. Solid line represents the least squares straight fitting data corresponding to  $\sigma = 0$ . Dashed lines join the noisy data for different values of  $\sigma$ , reaching the corresponding saturation label for small values of  $\epsilon$ . The rest of parameters are  $c = 0.6$ ,  $a = 1.1$  and  $d = 1.35$ .

$$\phi_l(l) = f \cdot \Phi(X(l, c)) \left[ aX(l, c)^3 + \epsilon X(l, c) \right]. \tag{31}$$

It is important to note that in this last equation, the function  $X(l, c)$  describing the linear phase of the intermittency, was derived without taking into account the effect of noise. This effect is only considered in Eq. (31) for the NRPD,  $\Phi(X(l, c))$ . In spite of that, the analytical description given by Eq. (31) approaches the numerical simulations very well as shown in Fig. 10 for type-II and type-III intermittency.

In absence of noise, the maps of Eqs. (1)–(3) exhibits the RPD given by Eq. (7). Recently it has been shown that for this RPD, the critical exponent  $\beta$  of the the characteristic relation  $\bar{l} \propto \epsilon^\beta$ , where  $\bar{l}$  is the average laminar length. Its value is determined by the slope of the function  $M(x)$  as follows [6]

$$\beta = \frac{\alpha + 2 - p}{p - 1} = \frac{1 + p(m - 1)}{(p - 1)(1 - m)}. \tag{32}$$

A log–log plot of the characteristic relation  $\bar{l} \propto \epsilon^\beta$  is shown by the solid lines in Figs. 11 and 12 when  $\sigma = 0$ . Note that for  $\sigma \neq 0$ , this characteristic relation and the numerical simulations are close for  $\epsilon > \sigma$ . On the contrary, for low values of  $\epsilon$ , ( $\epsilon < \sigma$ ), the time escape from the laminar region due to the dynamics of the map, as is described by Eq. (28), is shorter than the random escape. Hence, the escape speed is not practically influenced by a further decrease of  $\epsilon$  because it has a small effect on the random escape. As a consequence, the average laminar length,  $\bar{l}$ , reaches a saturation value. Note that this saturation value depends on the value of the noise strength  $\sigma$ , that governs the random speed in the laminar region, but also it depends on the NRPD that is generated during the chaotic phase and governs the starting point in the local map. This is clear in Fig. 11, since the local map where the laminar phase takes place is the same for the two cases shown in the figure. The value of noise strength  $\sigma$  is also the same, and the only difference is the parameter  $\gamma$  that determines the RPD in the noiseless case. Hence, contrary to what has been suggested [9,10], the average laminar length depends on the reinjection probability density.

#### 4. Conclusions

In this work we have extended to the noisy case some recent results proposed in [6,7]. Even though, there is certainly many papers devoted to the analysis of the effect of noise on the laminar region, to our knowledge, the effect of noise on the reinjection probability density (NRPD) has not been fully considered. In this work, we investigate this effect and we propose an analytical description of the noisy RPD (NRPD) valid for type-II and type-III intermittency.

To study the effect of noise we have used the methodology recently developed for the noiseless case [6,7]. That is, we start making a numerical evaluation of the function  $M(x)$ , that is easier to obtain than the reinjection probability density. From this knowledge, we obtain the reinjection probability density corresponding to the noiseless map, that is generated around the maximum and minimum of the map. We find that this mechanism is robust against noise, hence we can use the RPD to obtain an analytical description of the NRPD in a good agreement with numerical simulations. It is also important to note that from the RPD, obtained from noisy data, we have a complete description of the noiseless system.

Furthermore, we have found a good agreement between the analytical probability density of the laminar length and the numerical simulations. We show that for large values of  $\varepsilon$  compared to the noise strength,  $\varepsilon > \sigma$ , the characteristic relation approaches the noiseless prediction [6,7], whereas for  $\varepsilon < \sigma$  the average laminar length reaches a constant value that strongly depends on the NRPD and weakly on  $\varepsilon$ .

#### Acknowledgements

This research is supported the Spanish Ministry of Science and Innovation (MICINN) under Project No. FIS2010–20054 (EdR), Project No. FIS2009–09898 (MAFS) and the CONICET under Project No. PIP 11220090100809, and grants of the National University of Córdoba and MCyT of Córdoba, Argentina (SE).

#### References

- [1] Manneville P, Pomeau Y. *Phys Lett A* 1979;75:1.
- [2] Pomeau Y, Manneville P. *Commun Math Phys* 1980;74:189.
- [3] Chian A. *Complex Systems Approach to Economic Dynamics*. Berlin: Springer; 2007.
- [4] Zebrowski J, Baranowski R. *Physica A* 2004;336:74–83.
- [5] Schuster H, Just W. *Deterministic Chaos. An Introduction*. Weinheim, Germany: Wiley-VCH; 2005.
- [6] del Rio E, Elaskar S. *Int J Bifurcat Chaos* 2010;20:1185–91.
- [7] Elaskar S, del Rio E, Donoso JM. *Physica A* 2011;390:2759.
- [8] Hirsch JE, Nauenberg M, Scalapino DJ. *Phys Lett A* 1982;87:391.
- [9] Hirsch JE, Huberman BA, Scalapino DJ. *Phys Rev A* 1982;25:519.
- [10] Koronovskii AA, Hramov AE. *Eur Phys J B* 2008;62:447.
- [11] Kye WH, Rim S, Kim CM, Lee JH, Ryu JW, Yeom BS, et al. *Phys Rev E* 2003;68:036203.
- [12] Pikovsky AS. *J Phys A* 1983;16:L109.
- [13] Manneville P. *Le J de Physique* 1980;41:1235.